



Controlled three-dimensional immobilization of biomolecules on chemically patterned surfaces

A. Biebricher^a, A. Paul^b, P. Tinnefeld^a, A. Götzhäuser^{a,*}, M. Sauer^{a,1}

^a Fakultät für Physik, Universität Bielefeld, Universitätsstr. 25, 33615 Bielefeld, Germany

^b Ang. Phys. Chemie, Universität Heidelberg, INF 253, 69120 Heidelberg, Germany

Received 15 December 2003; received in revised form 15 March 2004; accepted 19 March 2004

Abstract

We used electron-beam lithography to fabricate chemical nanostructures, i.e. amino groups in aromatic self-assembled monolayers (SAMs) on gold surfaces. The amino groups are utilized as reactive species for mild covalent attachment of fluorescently labeled proteins. Since non-radiative energy transfer results in strong quenching of fluorescent dyes in the vicinity of the metal surfaces, different labeling strategies were investigated. Spacers of varying length were introduced between the gold surface and the fluorescently labeled proteins. First, streptavidin was directly coupled to the amino groups of the SAMs via a glutaraldehyde linker and fluorescently labeled biotin (X-Biotin) was added, resulting in a distance of ~ 2 nm between the dyes and the surface. Scanning confocal fluorescence images show that efficient energy transfer from the dye to the surface occurs, which is reflected in poor signal-to-background (S/B) ratios of ~ 1 . Coupling of a second streptavidin layer increases the S/B-ratio only slightly to ~ 2 . The S/B-ratio of the fluorescence signals could be further increased to ~ 4 by coupling of an additional fluorescently labeled antibody layer. Finally, we introduced tetraethylenepentamine as functional spacer molecule to diminish fluorescence quenching by the surface. We demonstrate that the use of this spacer in combination with multiple antibody layers enables the controlled fabrication of highly fluorescent three-dimensional nanostructures with S/B-ratios of >20 . The presented technique might be used advantageously for the controlled three-dimensional immobilization of single protein or DNA molecules and the well-defined assembly of protein complexes.

© 2004 Elsevier B.V. All rights reserved.

Keywords: Surface nanostructures; Electron-beam lithography; Chemical lithography; Scanning confocal fluorescence imaging; Self-assembled monolayers

1. Introduction

The development of techniques for the immobilization of biomolecules at the nanometer scale is an important area of research in nanotechnology (Whitesides et al., 2001; Willner and Katz, 2000). Controlled and accurate immobilization of a small number or even individual biomolecules at a

* Corresponding author. Tel.: +49-521-106-5362; fax: +49-521-106-6002.

E-mail addresses: goelzhaeuser@physik.uni-bielefeld.de (A. Götzhäuser), sauer@physik.uni-bielefeld.de (M. Sauer).

¹ Co-corresponding author. Tel.: +49 521 106 5451; fax: +49 521 106 2958.

specific location is also a key issue in biotechnology. Current methods include microcontact printing (μ CP) (James et al., 1998; Bernard et al., 1998), and dip-pen nanolithography (DPN) to deposit biological molecules at well defined positions on surfaces. Recently (Bruckbauer et al., 2002; Ying et al., 2002), a nanopipet in combination with scanning ion-conductance microscopy (SICM) was used to deposit biotinylated DNA on streptavidin coated cover slides or protein G on a positively charged glass surface with regular spot sizes of $\sim 1 \mu\text{m}$.

On the other hand, chemically defined surface nanostructures are advantageous as they offer laterally well defined sites at which biomolecules can be covalently attached to specific functional elements. Materials that are well suited to build surface nanopatterns are self-assembled monolayers (SAMs). SAMs are homogeneous, highly ordered films of organic molecules covalently anchored to a surface with a typical thickness of 1–2 nm and an intermolecular spacing of 0.5–1.0 nm (Ulman, 1998; Schreiber, 2000). SAMs are formed when surfactant molecules spontaneously adsorb in a monolayer on surfaces. The first and most widely studied systems of SAMs are alkylsilanes on SiO (Sagiv, 1980) and alkanethiols on gold (Nuzzo and Allara, 1983). In general, SAM systems can be tailored to bind to the surfaces of noble metals, semiconductors, and oxides. In biological applications, SAMs are frequently used as linkers to attach cells and proteins to surfaces (Mrksich, 1998).

One of the most powerful techniques to generate nanoscopic laterally patterned SAMs constitutes electron beam (e-beam) lithography (Lercel et al., 1996a,b; Harnett et al., 2000; Götzhäuser et al., 2000; Geyer et al., 2001). E-beams can be focused into very small spots ($< 1 \text{ nm}$) and e-beam lithography can produce precisely aligned patterns. Furthermore, e-beam lithography is easily combined with other microfabrication techniques. In e-beam lithography the resolution achievable is limited by the large size of the molecules in the polymeric resist and secondary electron processes such as forward scattering and proximity effect. However, these effects can be minimized by the use of small molecules, and SAMs have been successfully used to fabricate patterns with lateral sizes below 10 nm (Lercel et al., 1996a,b; Küller et al., 2003). Recently, a simple scheme to generate chemically distinct surface nanostructures based on SAMs has been demonstrated (Götzhäuser et al., 2001; Geyer et al., 2001). First, a densely packed monolayer of 4'-nitro-1,1'-biphenyl-4-thiol (NBT) was self-assembled on a gold surface. E-beam writing was used to locally modify the terminal nitro groups to amino groups (Eck et al., 2000), while the aromatic layer is dehydrogenated and cross linked (Geyer et al., 1999). Fig. 1 shows a schematic of these electron induced reactions that were characterized by X-ray photoelectron spectroscopy and near edge X-ray absorption spectroscopy (Geyer et al., 1999; Eck et al., 2000). The nitro-to-amino conversion can be performed with a yield of $\sim 90\%$, when applying

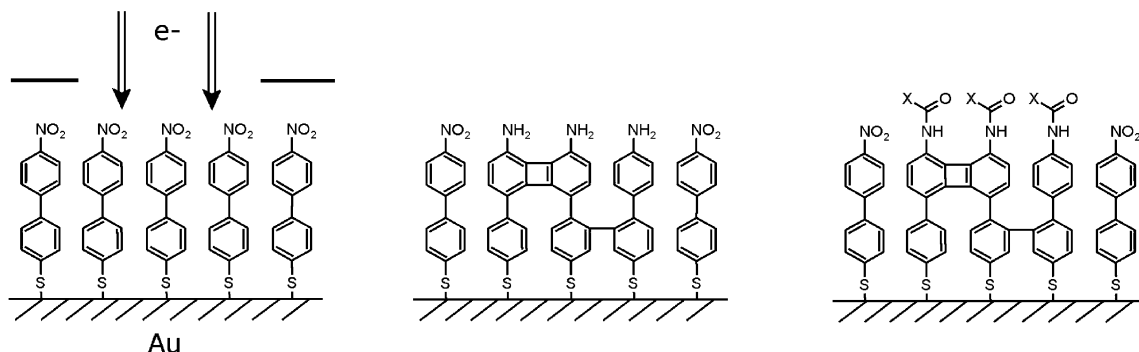


Fig. 1. Schematics of electron induced processes in NBT. A monolayer of NBT is irradiated by electrons and generates amino end groups while the underlying aromatic monolayer is dehydrogenated and cross linked. In a subsequent step the amino groups can be used for the mild covalent attachment of biomolecules.

an electron area dose of 40 mC/cm^2 . The generated well-ordered templates of amino groups can be used for specific covalent coupling of biomolecules using various spacer molecules.

For fluorescence-based applications of SAMs, quenching of the fluorophore by the gold surface has to be minimized. It is well known that excited-state lifetimes and consequently fluorescence intensities are abbreviated depending on the distance (within tens of nanometer) of fluorophores to metal surfaces due to fluorescence energy transfer to the metal (Kuhn, 1970; Chance et al., 1978; Whitmore et al., 1982; Kummerlen et al., 1993; Imahori et al., 2000; Yokota et al., 1998). Therefore, different strategies were evaluated to build three-dimensional protein and nucleic acid complexes which avoid direct contact of the fluorophores with the metal surface. Zhou et al. demonstrated for the first time fabrication of multi-layer bioassemblies on a surface at the micro–nano scale (Zhou et al., 2003). They used DNA and streptavidin/biotin as building blocks because DNA can be easily functionalized and different sequences can potentially be used for each layer to produce highly diverse structures. μCP was used to fabricate $2 \mu\text{m}$ SAM stripes on gold surfaces with biotin functionalities for the binding of streptavidin.

In this article, we use the specific reaction of NBT SAMs with electrons to build molecular surface nanostructures. E-beams directly create reactive surface sites, i.e. amino groups, for mild covalent immobilization of proteins. Nonspecific protein adsorption is prevented by binding of densely packed poly (ethylene glycol) to the remainder of the surface. As a proof of concept, we show that we can fabricate three-dimensional surface biological features through a templated sequential assembly of proteins and antibodies. Furthermore, our approach offers fine control over the pattern height which is crucial for fluorescence-based applications.

2. Materials and Methods

2.1. Chemicals

If not stated otherwise, all chemicals and solvents were purchased from Fluka (Germany), and used without further purification. Recombinant

streptavidin was purchased from Roche Diagnostics (Darmstadt, Germany). IgG-antibodies labeled with the two red dyes Alexa633 (Alexa633-IgG, excitation/emission maximum at 632/647 nm in water) and Alexa680 (Alexa680-IgG, excitation/emission maximum at 679/702 nm in water) were used as received (MoBiTec GmbH, Göttingen, Germany). For biotin/streptavidin studies, the activated dye (Cy5-*N*-hydroxy-succinimide; Amersham Pharmacia Biotech, Freiburg, Germany) was coupled to biotin cadaverine (Molecular Probes, Göttingen, Germany) in dimethylformamide with 1% *N*-diisopropylethylamine (Buschmann et al., 2003). The reaction solution was incubated for 90 min at room temperature and the product was purified by HPLC (Hewlett Packard, Böblingen, Germany) using a reversed-phase column (Knauer, Berlin, Germany) with octadecylsilan-hypersil C18. Separation was performed in 0.1 M triethylammonium acetate, using a linear gradient from 0 to 75% acetonitril in 20 min. Yields >80% were obtained.

2.2. SAM fabrication

NBT was synthesized according to the procedures described by Eck et al. (2000). Thirty nanometer gold films on a chromium primed (3 nm) silicon substrate were obtained from Albert coatings. NBT SAMs were produced by immersion of gold substrates in a degassed dimethylformamide solution for 72 h under nitrogen, followed by sonication, rinsing with ethanol, and drying under nitrogen flow.

2.3. Low energy electron proximity printing

Patterning of NBT SAMs with low energy electron proximity printing was performed in a high vacuum system at a base pressure of 10^{-7} mbar. The electrons were generated with a flood gun (Specs 15/40) placed ~ 4 cm from the sample surface with energies ranging from 50 to 500 eV. Carbon foils with well defined opening sizes from 1 to $4 \mu\text{m}$ (Quantifoil, Jena, Germany) were used as stencil masks. The NBT SAMs were exposed to area doses between 10 and 40 mC/cm^2 . A Faraday cup in the sample holder was used to measure the electron current during the irradiation.

2.4. Grafting with Poly (ethylene glycol)

Alkanethiol terminated poly (ethylene glycol) [HS(CH₂)₁₁(OCH₂-CH₂)_n-OCH₃, $n = 34-56$, MW ≈ 2224 Da] (PEG2000-SH) was synthesized according to the procedures described by (Tokumitsu et al., 2002). Layers of PEG2000-SH are grafted on gold surfaces by immersion of a gold substrate in 0.5 mM solution of PEG2000-SH in dimethylformamide solution for 12–24 h, followed by sonication, rinsing with ethanol, and drying under nitrogen flow. The (dry) thickness of the obtained PEG2000 graft varied from ~ 2 to 5 nm. Adsorbed PEG2000 prevents non-specific protein adsorption over a wide range of coverages and surface morphologies (Tokumitsu et al., 2002, Himmelhaus et al., 2003, Herrwerth et al., 2003).

2.5. Surface immobilization

All reactions were carried out at room temperature. Layers of protein were specifically bound to the irradiated and passivated surface. Cross linking was performed by incubation of the sample for 1 h in 10% glutaraldehyde, washing with water and drying. The activated surface was incubated for 1 h with protein in PBS. Next the sample was rinsed with 0.15% Tween20 in PBS, water and dried under nitrogen flow. For the first protein layer, 100 μ l of recombinant streptavidin at a concentration of 10 μ g/ml was applied. After cross linking, the surface was rinsed with 1% Tween20, PBS, and treated with 10^{-8} M Cy5-biotin without previous drying. After 45 min the surface was washed and dried under nitrogen flow. In an alternative experiment, streptavidin was incubated with Cy5-biotin (10^{-7} M) prior to binding to the surface.

For further modification of streptavidin coated surfaces, the dried protein layer was rehydrated before cross linking with glutaraldehyde in 0.15% Tween20 for 4 h. After a washing step and glutaraldehyde binding, 100 μ l of a 20 μ g/ml Alexa633-IgG solution was applied for 1 h. To further reduce nonspecific binding the solution contained 30% glycerol and 0.01% Tween20. Although further layers of protein could be coupled by reiteration of the procedure, accumulating non-specifically bound proteins led to decreasing S/B ratios after coupling.

In a second approach, the patterned SAMs were activated by treatment with 220 mg *p*-nitrophenylchloro-

formiate (NPCF) and 200 μ l *N*-diisopropyl-ethylamine in 15 ml 1,2-dichloroethane at room temperature for 2.5 h (Beier and Hoheisel, 1999). The sample was then thoroughly washed with dichloroethane, dried and immediately incubated overnight in 250 μ l tetraethylenepentaamine (TEPA) dissolved in 20 ml dimethylformamide. This was followed by rinsing with dimethylformamide, methanol and sonication for 15 min at 40 °C in the same solvent. Finally, the surface was washed with acetone and dried under nitrogen flow. Additional layers of TEPA were synthesized applying the same method. For protein cross linking to the bound TEPA, the sample was treated with 10% glutaraldehyde for 2.5 h, subsequently washed with water and dried, then incubated in 20 μ g/ml of Alexa-IgG with 30% glycerole and 0.01% Tween20 for 2.5 h. The reaction was terminated by washing with 0.05% Tween20, water, and drying under nitrogen. Further layers of Alexa-IgG were immobilized by sonication of the dried surfaces in 0.05% Tween 20 at 40 °C and incubation for 45 min. After rinsing with water and incubation in PBS for 24 h, cross linking was achieved according to the procedure above with the difference that only 15% glycerol was applied to the protein-solution without addition of Tween20.

2.6. Scanning Force Microscopy

Atomic force microscopy (AFM) was performed on a Solver P47H (NT-MDT, Moscow, Russia) equipped with a 50 μ m scanning device and the corresponding software. Measurements were done under air in the non-contact (NC)-mode using an aluminium-coated single-crystal silica point probe sensor (LOT-Oriel, Darmstadt). Typical cantilever specifications were: force constant of 42 N/m with resonance frequencies at 320 kHz, and a tip with a radius below 10 nm. For scanning, the sample was mounted on a glass plate. Scanning images are shown with the scanning size in *x,y*-direction as well as with the grayscale decoding the height.

2.7. Fluorescence Microscopy

The set-up for spectrally-resolved fluorescence imaging microscopy is described in detail elsewhere (Tinnefeld et al., 2001). For excitation a pulsed diode

laser with a center wavelength of 635 nm, a repetition rate of 32 MHz, and a pulse length of less than 100 ps (PDL800B; Picoquant, Berlin, Germany) was used. Passing an excitation filter (639DF9; Omega Optics, Brattleboro, VT) the collimated laser beam was directed into an inverted microscope (Axiovert 100TV; Zeiss, Germany) via the backport and coupled into an oil immersion objective (100 \times , NA = 1.4; Nikon, Japan) by a dichroic beam splitter (645DMLP; Omega Optics, Brattleboro, VT). Fluorescence light was collected with the same objective and focused through the TV-outlet of the microscope onto a 100 μ m pinhole. Fluorescence light passing the pinhole was spectrally filtered by a long pass filter 650 CFLP (Chroma Technology Corp., Rockingham, VT), separated by a dichroic beam splitter (685DFLP; Omega Optics, Brattleboro, VT), and imaged onto the active areas of two avalanche photodiodes (AQR-14; EG&G, Canada). The reflected fluorescence intensity reaching detector 1, I_1 , and transmitted fluorescence intensity reaching detector 2, I_2 , were filtered with appropriate bandpass filters (667DF30 and 710DF50; Chroma Technology Corp., Rockingham, VT). For the generation of spectrally-resolved fluorescence intensity images the microscope was equipped with a piezoelectric x,y -scanning device (Physik Instrumente, Karlsruhe, Germany). The signals of the two APDs were fed into the router of a TCSPC PC interface card (SP-630; Becker&Hickl, Berlin, Germany) to acquire time-resolved data. For synchronization of scanning and time-correlated single-photon counting, a LabView 6.0-based software was developed. Imaging was performed by placing the sample upside down on a glass coverslip (50 mm \times 24 mm \times 0.17 mm; Roth, Karlsruhe, Germany).

Scanning was performed in two modes, either “overview”-mode (50 μ m \times 50 μ m, 250 nm/pixel) or “detail”-mode (20 μ m \times 20 μ m, 50 nm/pixel) with a constant integration time of 3 ms/pixel. The laser excitation intensity at the sample was varied over a broad range from 100 W/cm² to 12 kW/cm² depending on the fluorescence intensity of the sample, and adjusted to provide the best signal/background (S/B)-ratio. Statistical analysis of the patterned surfaces was done using a home built program selecting \sim 50 fluorescent spots from different scans of the same sample. Average count rates per pixel detected within 1.5 μ m

circles from fluorescent spots and background were used to calculate the S/B ratio.

3. Results and discussion

To covalently attach proteins to the amino-modified regions (1.5 μ m circles) of e-beam patterned NBT-SAMs, we used glutaraldehyde as cross linker (Hermanson, 1996). Though the resulting imine bond is known to be labile in aqueous solutions, no significant detachment of proteins from the surface was observed in the reactions described. Because of the strong binding of up to four biotin molecules to the 60 kDa protein streptavidin ($K_D = 10^{-15}$ M) it was used as simple model system in the first experiments (Weber et al., 1989; Chevalier et al., 1997). The samples were then treated with streptavidin to produce a structured protein surface. Binding of streptavidin to the irradiated regions was investigated by non-contact AFM which shows 1.5 μ m structures with a height of \sim 2 nm (not shown). The increase in height is less than expected for adding a densely packed monolayer of streptavidin (5 nm) (Riepl et al., 2002). A possible explanation is the relatively low surface coverage achievable for the first streptavidin layer, and the embedding of streptavidin in the surrounding PEG2000. However, the value is in the range commonly observed in AFM measurements of similar proteins (Cherny et al., 1998; Woolley et al., 2000; Zhou et al., 2003). Since each streptavidin molecule has four binding sites, two on each side of the protein, the upper ones should be available for binding of fluorescently labeled biotins. Scanning confocal fluorescence images recorded after treatment with Cy5-biotin (not shown) show a very poor S/B ratio (\sim 1.2) and thus demonstrate that the fluorescence intensity of the fluorophore is drastically reduced due to efficient energy transfer to the gold surface.

To increase the distance between the fluorophore and the Au surface, we have chosen proteins, e.g. streptavidin or antibodies, as universal building blocks. The basic idea behind is that almost any protein layer offers a huge number of lysine residues with aliphatic amino groups on its core which can be further cross linked by glutaraldehyde. Thus, each protein layer serves as an additional spacer in the order of several nanometers, thereby reducing the

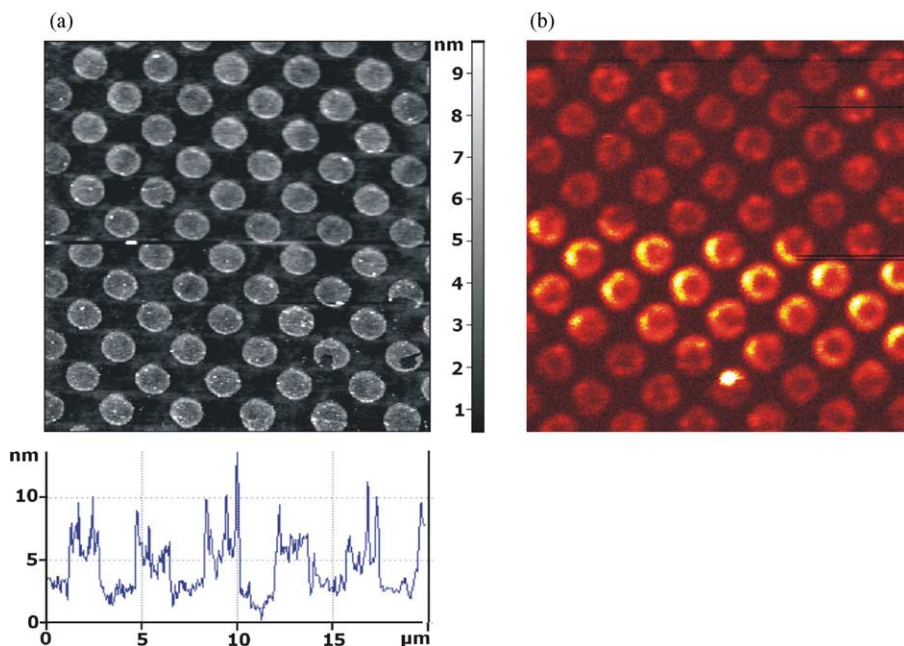


Fig. 2. AFM (a) and fluorescence intensity image (b) ($20\ \mu\text{m} \times 20\ \mu\text{m}$, $100\ \text{kW}/\text{cm}^2$, intensity scale: 0–180 counts/3 ms) of streptavidin treated $1.5\ \mu\text{m}$ patterns generated by e-beam lithography in NBT after cross linking with a second layer of Cy5-biotin labeled streptavidin. The height of the protein spots is $\sim 4\ \text{nm}$ and nonspecific adsorption of proteins on the surface is very low. The fluorescent spots show S/B-ratios ~ 2 .

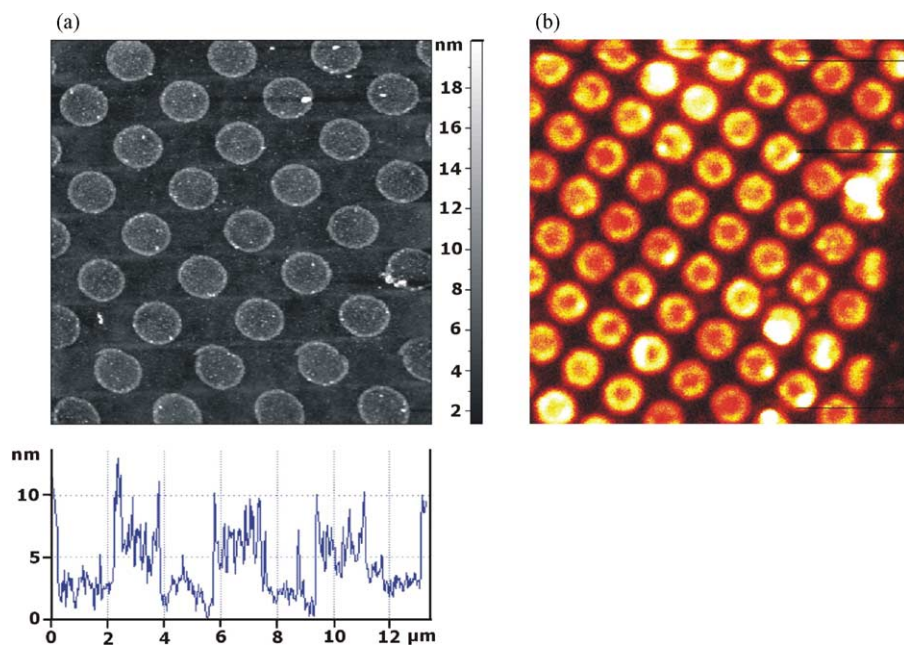


Fig. 3. AFM: (a) and fluorescence intensity image; (b) ($20\ \mu\text{m} \times 20\ \mu\text{m}$, $100\ \text{kW}/\text{cm}^2$, intensity scale: 0–180 counts/3 ms) of the same surface as shown in Fig. 2 after treatment with a third protein layer of Alexa633-IgG.

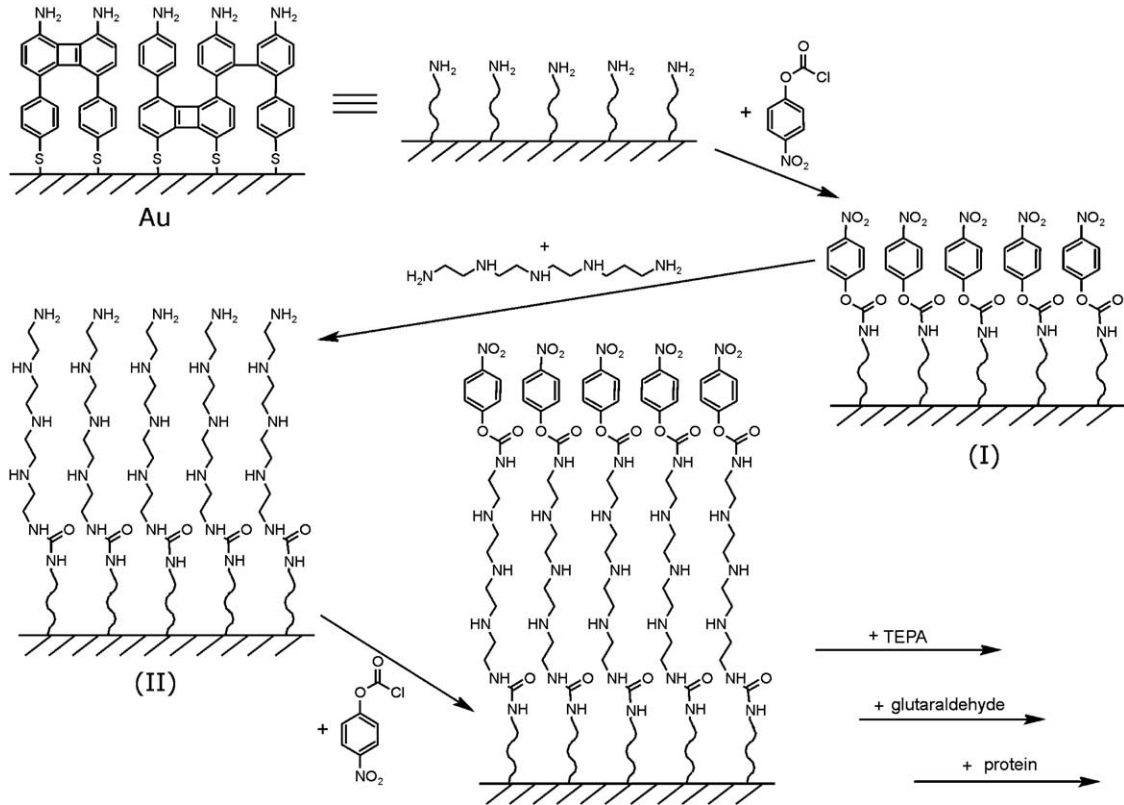


Fig. 4. Schematic of fabrication of three-dimensional fluorescently labeled biological assemblies on the nanometer scale. The amino-groups in the irradiated spots can first be modified with an aminolinker by activation with NPCF. The activated surface (I) can subsequently form a stable urea-bond with TEPA. The new surface (II) exhibits also amino-groups and can again be reacted with NPCF and TEPA. Finally, the top amino-layer is treated with glutaraldehyde and cross linked with protein. These steps can be repeated to further increase the distance to the surface. Alternatively, the top layer can be cross linked with a protein which also exhibits amino groups (lysine residues) at its core facilitating immobilization of further protein layers.

fluorescence quenching efficiency. For example, for each streptavidin layer an increase in distance of ~ 2 nm is expected. Therefore, we coupled a second streptavidin layer on top of the first. Here, the streptavidin was already incubated with Cy5-biotin prior to coupling. The successful coupling of streptavidin labeled with Cy5-biotin on an existing streptavidin layer was demonstrated by AFM which shows a significant increase in the height of the protein pattern (Fig. 2a). Due to the increased distance from the surface (~ 4 nm), quenching via energy transfer to the metal surface is reduced (Fig. 2b). Using the double-layer strategy S/B ratios of ~ 2 are obtained. As can be seen by both the AFM and the fluorescence image, the protein density within the spots appears heterogeneous. The highest protein density appears

at the rims of the spots. Even under various coupling conditions, the surface coverage for the first protein layer is the highest at the rims of the spots.

To further increase the distance to the surface, the protein pattern was treated with a third protein, a fluorescently labeled antibody (Alexa633-IgG). Here, glycerol and Tween20 were added to minimize nonspecific adsorption of antibodies on the surface without interfering with the chemical reactivity. Both the distance to the surface, i.e. the height of the protein structure, and the fluorescence intensity increase significantly to ~ 6 nm (Fig. 3a), with S/B ratios of ~ 4 (Fig. 3b). Again, the rims of the spots are clearly visible due to the increased protein density.

The results obtained demonstrate that it would be advantageous to combine the protein coupling

cycle strategy with a more potent spacer which is compatible with specific protein cross linking to achieve higher S/B ratios in the corresponding fluorescence images. Therefore, we used the spacer system *p*-nitrophenylchloroformiate (NPCF) and tetraethylenepentamine (TEPA) known from DNA-array immobilization (Fig. 4) (Beier and Hoheisel, 1999). This system provides several distinct advantages, as there are easy modification procedures and a higher reactivity of NPCF with amino groups as compared to glutaraldehyde. The reactivity of the spacer system is of fundamental importance since it is very likely that the irradiated SAMs exhibit a significant number of enamines and/or aromatic amines which do not react efficiently with aldehydes, e.g. glutaraldehyde. On the other hand, acidchlorides, such as NPCF, are known to react with aromatic amines. Furthermore, TEPA exhibits a 11-atom-chain between the primary amines which makes it well suited as an efficient spacer. Since we could not get satisfactory AFM images of the surfaces treated with NPCF and TEPA, the conformation of the penta-amino linker on the surface remains speculation. However, considering the density of potential binding sites and reactivity, a stretched layer should be preferred because of steric hindrance. In addition, stabilization of the secondary amines by mutual hydrogen-bond formation seems possible. A further advantage arises from the fact that it has to be considered that each chemical reaction has a yield of <100% which results in a decrease in surface coverage with each immobilization step. Here, the use of TEPA is also advantageous because each molecule exhibits four potential binding sites, i.e. amino groups (though not all of them are probably accessible in a dense layer) for coupling of the next protein layer.

Indeed, we found a dramatic increase in fluorescence intensity compared to directly immobilized proteins after cross linking of Alexa633-IgG molecules to a surface solely modified with a single layer of TEPA (data not shown). Using two TEPA layers and a single Alexa633-IgG layer, the fluorescence intensity images exhibit S/B ratios of ~20, i.e. a considerable increase as compared to the direct immobilization strategy (Fig. 5). In addition, the surface coverage is far more homogenous within the spots. In the following experiments we tried to couple an additional

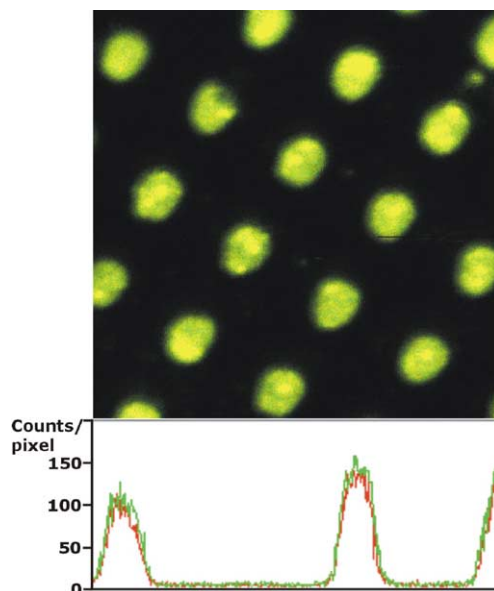


Fig. 5. Overall false-color fluorescence intensity image ($20\ \mu\text{m} \times 20\ \mu\text{m}$, $1.2\ \text{kW}/\text{cm}^2$, intensity scale: 0–100 counts/3 ms) of two layers of TEPA cross linked with one layer of Alexa633-IgG. The fluorescence intensity increased dramatically yielding a S/B-ratio ~20. As expected for Alexa633 with a fluorescence emission maximum at ~650 nm, the yellow-green color of the spots indicates comparable intensities recorded on Det1 (green) and Det2 (red). This can be directly seen in the line scan image (below).

antibody layer carrying a different fluorescent dye on top of the protein pattern. After activation of the previous antibody with glutaraldehyde, the sample was treated with the second antibody Alexa680-IgG. Using spectrally-resolved fluorescence imaging with a dichroic beam splitter at 685 nm, the fluorescence of the Alexa633 labeled antibody with an emission maximum at ~650 nm is detected predominantly on the short-wavelength detector (Det1), while the emission of the second antibody layer (Alexa680 labeled antibody) is detected exclusively on the long-wavelength detector (Det2). From the ratio of the fluorescence signals recorded on the two detectors we calculate the fractional intensity, F_2 , detected at Det2 according to $F_2 = I_{\text{Det2}} / (I_{\text{Det1}} + I_{\text{Det2}})$. From the knowledge of the transmission curves of the filters used and fluorescence emission curves recorded from ensemble measurements we expect F_2 -values of ~0.4 for Alexa633-IgG, and ~0.9 for Alexa680-IgG. Fig. 6a

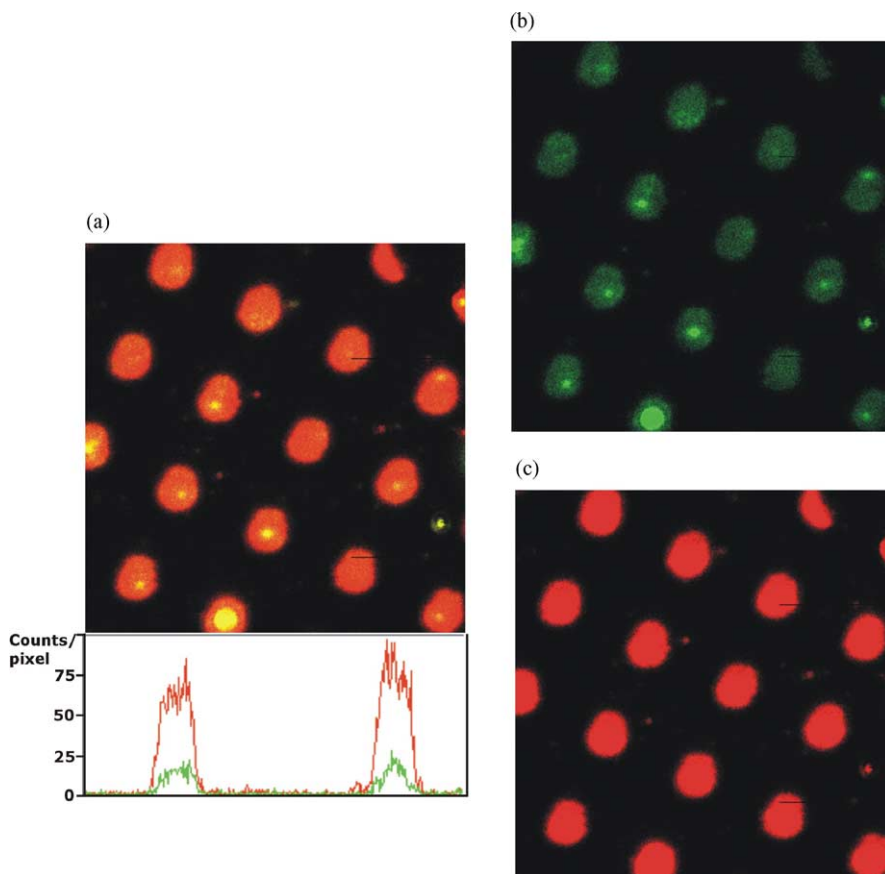


Fig. 6. (a) False-color fluorescence intensity image ($20\ \mu\text{m} \times 20\ \mu\text{m}$) of the surface shown in Fig. 5 cross linked with an additional layer of Alexa680-IgG applying a ~ 10 -fold lower excitation intensity ($120\ \text{W}/\text{cm}^2$). The image is reconstructed from the two fluorescence intensity images recorded at the short-wavelength detector, Det1 (green) (b); and long-wavelength detector, Det2 (red) (c). The line scan demonstrates that the overall fluorescence intensity is dominated by the second antibody Alexa680-IgG. The higher fluorescence intensities recorded on Det2 are reflected in high F_2 -values of ~ 0.8 . That is, the different fluorescence intensities directly correlate with the distance of the fluorophores to the Au surface.

shows a false-color fluorescence image constructed from the overall fluorescence intensity recorded at Det1 and Det2 after immobilization of the second antibody layer Alexa680-IgG. While the fluorescence spots measured from the surface carrying only the first antibody layer with Alexa633-IgG (Fig. 5) exhibit F_2 -values of ~ 0.4 , the fluorescent spots in Fig. 6 show average F_2 -values of ~ 0.8 with a S/B ratio of ~ 25 under lower excitation intensity. The strong increase in fluorescence intensity (compare Fig. 6b and c) and the shift of the F_2 -value from ~ 0.4 to 0.8 upon coupling of the second antibody layer (Alexa680-IgG) together

with the fact that Alexa680 exhibits a lower fluorescence quantum yield than Alexa633 under aqueous conditions, demonstrates that the increase in fluorescence intensity is a result of diminished fluorescence quenching, i.e. a larger distance of the fluorophore to the Au surface. Although, a reduction in quenching efficiency is expected to result also in a longer fluorescence lifetime, the fluorescence decays recorded on the two detectors were still too short to be resolved with the set-up used to measure time-resolved data with an instrument response function of $\sim 350\ \text{ps}$ (FWHM).

Acknowledgements

We thank V. Buschmann (Florida State University) for providing the Cy5 derivative Cy5-biotin, W. Eck (Universität Heidelberg) for providing us with NBT and PEG2000, and B. Holzapfel (Universität Marburg) for help with the SAM preparation. This work was supported by the BMBF (Grants 311864 and 13N8352) and the DFG.

References

- Beier, M., Hoheisel, J.D., 1999. Versatile derivatisation of solid support media for covalent bonding on dna-microchips. *Nucleic Acids Res.* 27, 1970–1977.
- Bernard, A., Delamar, E., Schmid, H., Michel, B., Bosshard, H.R., Biebuyck, H., 1998. Printing patterns of proteins. *Langmuir* 14, 2225–2229.
- Bruckbauer, A., Ying, L., Rothery, A.M., Zhou, D., Shevchuk, A.I., Abell, C., Korchev, Y.E., Klenerman, D., 2002. Writing with DNA and protein using a nanopipet for controlled delivery. *J. Am. Chem. Soc.* 124, 8810–8811.
- Buschmann, V., Weston, K.D., Sauer, M., 2003. Spectroscopic study and evaluation of red-absorbing fluorescent dyes. *Bioconjugate Chem.* 14, 195–204.
- Chance, R., Prock, A., Silbey, R., 1978. Molecular fluorescence and energy transfer near interfaces. In: Prigogine, I., Rice, S.R. (Eds.), *Adv. Chem. Phys.* 37, Wiley, New York, pp. 1–60.
- Cherny, D.I., Fourcade, A., Svinatchuk, F., Nielsen, P.E., Malvy, C., Delain, E., 1998. Analysis of various sequence-specific triplexes by electron and atomic force microscopy. *Biophysical J.* 74, 1015–1023.
- Chevalier, J., Yi, J., Michel, O., Ming, T.X., 1997. Biotin and digoxigenin as labels for light and electron microscopy in situ hybridization probes: where do we stand? *J. Histochem. Cytochem.* 45, 481–491.
- Eck, W., Stadler, V., Geyer, W., Zharnikov, M., Götzhäuser, A., Grunze, M., 2000. Generation of surface amino groups on aromatic self-assembled monolayers by low energy electron beams: a first step towards chemical lithography. *Adv. Mater.* 13, 806–808.
- Geyer, W., Stadler, V., Eck, W., Zharnikov, M., Götzhäuser, A., Grunze, M., 1999. Electron induced cross-linking of aromatic self-assembled monolayers: negative resists for nanolithography. *Appl. Phys. Lett.* 75, 2401.
- Geyer, W., Stadler, V., Eck, W., Götzhäuser, M., Sauer, M., Weimann, T., Hinze, P., 2001. Electron induced chemical nanolithography with self-assembled monolayers. *J. Vac. Sci. Technol. B* 19, 2732–2735.
- Götzhäuser, A., Geyer, W., Stadler, V., Eck, W., Grunze, M., Edinger, K., Weimann, T., Hinze, P., 2000. Patterning self-assembled monolayers with electrons. *J. Vac. Sci. Technol. B* 18, 3414–3418.
- Götzhäuser, A., Eck, W., Geyer, W., Stadler, V., Weimann, T., Hinze, P., Grunze, M., 2001. Chemical nanolithography with electron beams. *Adv. Mater.* 13, 806–809.
- Harnett, C.K., Satyalakshmi, K.M., Craighead, H.G., 2000. Electron-beam patterning of amine-functionalized self-assembled monolayers. *Appl. Phys. Lett.* 76, 2466–2468.
- Hermanson, G. T., 1996. Homobifunctional Cross-Linkers. In *Bioconjugate Techniques*, Academic Press., San. Diego, California, pp. 219–220.
- Herrwerth, S., Eck, W., Reinhard, S., Grunze, M., 2003. Factors that determine the protein resistance of oligoether self-assembled monolayers—internal hydrophilicity, terminal hydrophilicity, and lateral packing density. *J. Am. Chem. Soc.* 125, 9359–9366.
- Himmelhaus, M., Bastuck, T., Tokumitsu, S., Grunze, M., Livadaru, L., Kreuzer, H.J., 2003. Growth of a dense polymer brush layer from solution. *Europhys. Lett.* 64, 378–384.
- Imahori, H., Norieda, H., Nishimura, Y., Yamazaki, I., Higuchi, K., Kato, N., Motohiro, T., Yamada, H., Tamaki, K., Arimura, M., Sakata, Y., 2000. Chain length effect on the structure and photoelectrochemical properties of self-assembled monolayers of porphyrins on gold electrodes. *J. Phys. Chem. B* 104, 1253–1260.
- James, C.D., Davis, R.C., Kam, L., Craighead, H.G., Isaacson, M., Turner, J.N., Shain, W., 1998. Patterned protein layers on solid substrates by thin stamp microcontact printing. *Langmuir* 14, 741–744.
- Kuhn, H., 1970. Classical aspects of energy transfer in molecular systems. *J. Chem. Phys.* 53, 101–108.
- Küller, A., Eck, W., Stadler, V., Geyer, W., Götzhäuser, A., 2003. Nanostructuring of silicon by electron-beam lithography of self-assembled hydroxybiphenyl monolayers. *Appl. Phys. Lett.* 82, 3776.
- Kummerlen, J., Leitner, A., Brunner, H., Aussenegg, F.R., Wokaun, A., 1993. Enhanced Dye Fluorescence over Silver Island Films: Analysis of Distance Dependence. *Mol. Phys.* 80, 1031–1046.
- Lercel, M.J., Whelan, C.S., Craighead, H.G., Seshadri, K., Allara, D.L., 1996a. Plasma etching with self-assembled monolayer masks for nanostructure fabrication. *J. Vac. Sci. Technol. B* 14, 1844–1849.
- Lercel, M.J., Craighead, H.G., Parokh, A.N., Seshadri, K., Allara, D.L., 1996b. Sub-10 nm lithography with self-assembled monolayers. *Appl. Phys. Lett.* 68, 1504–1506.
- Mrksich, M., 1998. Tailored substrates for studies of attached cell culture. *Cell. Mol. Life Sci.* 54, 653–662.
- Nuzzo, R.G., Allara, D.L., 1983. Adsorption of bifunctional organic disulfides on gold surfaces. *J. Am. Chem. Soc.* 105, 4481–4483.
- Riepl, M., Enander, K., Liedberg, B., Schäferling, M., Kruschina, M., Ortigao, F., 2002. Functionalized surfaces of mixed alkanethiols on gold as a platform for oligonucleotide microarrays. *Langmuir* 18, 7016–7023.
- Sagiv, J., 1980. Organized monolayers by adsorption. I. formation and structure of oleophobic mixed monolayers on solid surfaces. *J. Am. Chem. Soc.* 102, 92–98.

- Schreiber, F., 2000. Structure and growth of self-assembling monolayers. *Prog. Surf. Sci.* 65, 151–256.
- Tinnefeld, P., Herten, D.P., Sauer, M., 2001. Photophysical dynamics of single dye molecules studied by spectrally-resolved fluorescence lifetime imaging microscopy (SFLIM). *J. Phys. Chem. A* 105, 7989–8003.
- Tokumitsu, S., Liebich, A., Herrwerth, S., Eck, W., Himmelhaus, M., Grunze, M., 2002. Grafting of alkanethiol-terminated poly (ethylene glycol) on gold. *Langmuir* 18, 8862–8870.
- Ulman, A., 1998. Formation and structure of self-assembled monolayers. *Chem. Rev.* 96, 1533–1554.
- Weber, P.C., Ohlendorf, D.H., Wendolowski, J.J., Salemme, F.R., 1989. Structural origins of high-affinity biotin binding to streptavidin. *Science* 243, 85–88.
- Whitesides, G.M., Ostuni, E., Takayama, S., Jiang, X., Ingber, D.E., 2001. Soft lithography for biology. *Annu. Rev. Biomed. Eng.* 3, 335–373.
- Whitmore, P.M., Robota, H.J., Harris, C.B., 1982. Electronic energy transfer from pyrazine to a silver(111) surface between 10 and 400 Å. *J. Chem. Phys.* 73, 740–741.
- Willner, I., Katz, E., 2000. Integration of layered redox proteins and conductive supports for bioelectronic applications. *Angew. Chem. Int. Ed.* 39, 1180.
- Woolley, A.T., Guillemette, C., Cheung, C.I., Housman, D.E., Lieber, C.M., 2000. Direct haplotyping of kilobase-size DNA using carbon-nanotube probes. *Nat. Biotechnol.* 18, 760–763.
- Ying, L., Bruckbauer, A., Rothery, A.M., Korchev, Y.E., Klenerman, D., 2002. Programmable delivery of DNA through a nanopipet. *Anal. Chem.* 74, 1380–1385.
- Yokota, H., Saito, K., Yanagida, T., 1998. Single molecule imaging of fluorescently labeled proteins on metal by surface plasmons in aqueous solution. *Phys. Rev. Lett.* 80, 4606–4609.
- Zhou, D., Bruckbauer, A., Ying, L., Abell, C., Klenerman, D., 2003. Building three-dimensional surface biological assemblies on the nanometer scale. *Nano Lett.* 3, 1517–1520.